Journal of Materials Processing Tech. 298 (2021) 117313

Contents lists available at ScienceDirect

Journal of Materials Processing Tech.

journal homepage: www.elsevier.com/locate/jmatprotec

Influence of surface integrity induced by multiple machining processes upon the fatigue performance of a nickel based superalloy

Zhirong Liao [a], Dongdong Xu [a], Gonzalo García Luna [a], Dragos Axinte [a,*], Giedrius Augustinavicius [b], Jon Ander Sarasua [c], Anders Wretland [d]

[a] Machining and Condition Monitoring Group, Faculty of Engineering, University of Nottingham, UK
[b] Waterjet AG, Switzerland
[c] IK4-TEKNIKER, Polo Tecnológico de Eibar, c/Iñaki Goenaga 5, Eibar, Guipuzcoa, Spain
[d] GKN Aerospace Engine Systems, Sweden

ARTICLE INFO

Associate Editor: E. Budak

Keywords:
Nickel based superalloy
Machining
Surface integrity
Fatigue
Fractography

ABSTRACT

Machining operations are of key importance to the fatigue performance of nickel based superalloys due to the high thermal/mechanical loadings yielded on the machined workpiece which can significantly alter the surface integrity of the components. Therefore, understanding the influence mechanisms of machining induced surface integrity upon fatigue response is vital to determine their manufacturing processes and applications. In this respect, this paper investigates the surface integrity of nickel based superalloy subject to different mechanical and thermal loadings induced by various machining processes including conventional machining (e.g. finish and rough milling) and nonconventional machining (e.g. laser assisted milling and abrasive waterjet cutting) methods, as well as their influences upon fatigue performance and failure mechanisms. In-depth surface metallurgical and crystallographic analysis has been conducted to reveal the surface damage mechanisms, which allows the description of the machining induced mechanical and thermal alterations on the machined workpiece. Furthermore, the examination of the fractography from the fatigue specimen has been conducted, which enables the understanding of the influence mechanism of the corresponding surface defects on the fatigue crack initiation and propagation, subject to a four points bending fatigue test. While the resulted S-N curves indicate that the high cycle fatigue of machined nickel based superalloy is mainly dominated by the machining induced residual stress conditions, the surface defects from different machining processes can particularly influence fatigue crack initiation and propagation mechanisms in both the low and high cycle regimes.

1. Introduction

Considering the extremely high thermo-mechanical loadings at which aeroengines run, materials with exclusive combination of mechanical properties at elevated temperatures, e.g. nickel based superalloy, have been extensively used for manufacturing the safety-critical components (Chaabani et al., 2020; Xu et al., 2020a). However, Toubhans et al. (2020) demonstrated that these materials, with their specific solid solution strengthening and precipitation hardening effects, have a particularly low machinability which results in poor surface integrity and reduced functional performances. It has been reported that the high mechanical and thermal loadings induced by the conventional machining processes can lead to a rapid tool wear and severely damaged surface and eventually deteriorate their functional performances (Holmberg et al., 2021; Huang and Yan, 2020). Hence, Liao et al. (2018) proposed that relatively conservative cutting parameters (e.g. low material removal rate) should be employed for the finishing operations to surmount these challenges, which however also leads to time-consuming and cost-inefficient outcomes.

To tackle with these challenges, particular non-conventional machining operations that can increase the material removal rate have also been proposed, such as abrasive waterjet (AWJ) machining (Suárez et al., 2019; Diaz et al., 2019) and laser assisted machining (LAM) (Oh et al., 2018; Liao et al., 2019). For instance, AWJ machining yields very low cutting forces and avoids the direct contact with a "hard" (solid) tool (Nguyen et al., 2020) while the LAM process can pre-soften the workpiece materials to be removed thus leading to significantly improve machinability. However, with their specific material removal

* Corresponding author.
E-mail address: Dragos.Axinte@Nottingham.ac.uk (D. Axinte).

https://doi.org/10.1016/j.jmatprotec.2021.117313
Received 16 April 2021; Received in revised form 12 July 2021; Accepted 13 July 2021
Available online 29 July 2021

mechanisms, these processes naturally lead to the unique surface integrity. Specifically, Liao et al. (2020) reported that AWJ machined surface presents a large number of scratches and grit embedment that can act as stress concentration sites when machined parts are subjected to mechanical loadings. For the LAM process, although relatively high metallurgical surface integrity has been achieved by Shang et al. (2019), Xu et al. (2020b) reported that the machined surface displays high tensile residual stresses due to the significant thermal energy that has been induced in the workpiece material. These surface/subsurface alterations have been chiefly of concern for the functional performance of the machined parts, especially those employed in key safety-critical applications (e.g. nuclear, aerospace). In this context, outstanding progress in the microstructural analysis of surface integrity has been made by Devillez et al. (2011) to support the optimisation of the conventional machining processes. Nevertheless, on one hand, non-conventional machining methods have been developed to provide an improved machinability a broad of materials, e.g. metals (Chrysolouris, 1997), composites (Dandekar and Shin, 2010) and ceramics (Tian and Shin, 2007); on the other hand, in spite of the substantial advances on the analysis of surface integrity, in-depth understanding of the thermal/mechanical loading imposed by machining processes on the material failure mechanisms of machined components, e.g. fatigue, is still lacking.

Fatigue crack, namely a critical material failure mechanism through the micro crack initiation and rapid propagation under cyclic loading, has been identified as one of the key performances to be considered in relation to safety cautious engineering (Xu et al., 2018). It is believed that the fatigue performance of machined workpiece is specifically sensitive to its surface integrity (Ezugwu et al., 2003) because the superficial layer experiences severe mechanical and/or thermal loadings, that alters the initial material properties, which, in turn, would affect the part's ability to withstand the working conditions (Kosai and Yan, 2020). Although it has been recognised the importance to investigate how the surface generation mechanism of the machined parts can affect their fatigue performance, most research focused on the relationship between the cutting conditions and fatigue life (Wu et al., 2018). Moreover, very little attention has been paid to the crack initiation and growth mechanisms that are in intimate relationships with the micro alterations of the workpiece surface after machining (Umbrello and Rotella, 2018). Hence, the nature of thermal and mechanical loadings experienced by workpiece subsurface under different machining methods (e.g. conventional and non-conventional machining) and their impact on fatigue performance is not very well understood, despite their key relationship with the microstructural alterations induced in the workpiece subsurface.

In fact, as reported by Herbert et al. (2014) and Holmberg et al. (2021), the nickel based superalloy can undergo significant mechanical and/or thermal loadings in both conventional and non-conventional machining processes, which results in particular metallurgical and mechanical alterations, while its fatigue performance can be considerably influenced. As such, it is difficult to select the appropriate methods from the current available machining processes to make full use of their advantages to arrange the best manufacturing route (Davis et al., 2020; Yang et al., 2020). Consequently, although these non-conventional methods have shown great potential on machining difficult-to-cut materials (Liu et al., 2020a,b), their use on the final machining stages of safety-critical parts, whereby the influence mechanism on the fatigue failure from the machining induced surface alteration reminds unclear, has not yet been clearly addressed (Deng et al., 2020).

Therefore, in the present research, the machined workpieces (i.e. Inconel 718) from both conventional and non-conventional machining methods have been investigated to understand the generation of surface (e.g. metallurgical and mechanical) alterations and their influences on the fatigue failure mechanism. This will include mechanically dominated processes, i.e. conventional finish milling (CFM) and abrasive waterjet cutting (AWJ), and combined mechanical and thermal dominated processes, i.e. conventional rough milling (CRM) and laser assisted milling (LAM). A series of 4 points bending fatigue tests were conducted under different loading levels, that include both plastic and elastic deformation regimes, to support the understanding of their fatigue performance in relation to the surface loading history (e.g. mechanical and thermal) imposed by these machining processes. Furthermore, an in-depth microstructural fractography has also been investigated to reveal the influence of fatigue crack initiation and propagation mechanisms from different surface defects. As such, the present investigation will allow the fundamental understanding of the influences of diverse loadings from different machining processes on the corresponding surface alterations and their further impacts upon the part's fatigue performance.

2. Materials and methodology

2.1. Rationale of selecting conventional and non-conventional methods in studying surface integrity effect upon fatigue performance

To investigate the influence of mechanical and thermal loadings upon the fatigue failure mechanism of the machined workpiece, both conventional (e.g. finish and rough milling) and non-conventional (AWJ and LAM) machining processes have been employed in this work to manufacture the workpiece for 4 points bending fatigue test with a final dimension of 6 mm x 6 mm x 100 mm, as shown in Fig. 1(d).

In this context, laser assisted machining (LAM) is proposed to enable local preheating of the workpiece ahead of the cutter by the laser beam to soften the material to be removed, and eventually improve the machinability of difficult-to-cut materials, i.e. in this case Inconel 718. As shown in Fig. 1(a), a recently developed method for smart control of beam scanning (based on solving the inverse problem in heat placement (Shang et al., 2018)) was applied in the present research to uniformly heat the workpiece ahead of the cutting tool at a particular temperature and depth below the free surface (i.e. 800 °C) to enable reduction of material strength and, therefore, increased machinability (Shang et al., 2019). However, as high external thermal energy is induced into the workpiece, how this can affect the fatigue failure mechanism of nickel based superalloy is still not clear. Hence, to understand the hybrid thermal and mechanical impact on the machined surface with its influence to fatigue failure mechanism, the above mentioned LAM method has been employed to prepare the fatigue test sample. As a comparison, the conventional machining processes, e.g. rough and finish milling (Fig. 1b), have also been investigated, whereby different levels of mechanical and thermal influences can be achieved through the controlled cutting parameters.

On the other hand, the principle of abrasive waterjet machining, i.e. mechanical material removal, is to erode the workpiece material by the impact of multiple high velocity (e.g. 300–700 m/s) abrasive particles enabled by the use of high pump pressure (e.g. ~400 MPa), as shown in Fig. 1(c), which can result in a compressive residual stress with material plastic deformation on the workpiece surface and the superficial layer (Liao et al., 2020). In this context, despite the obvious advantages mentioned before (very low cutting force, negligible heat-affect areas and comparatively high material removal rates), the significant amount of scratches and abrasive embedment on the machined surface rise the safety concern when manufacturing the high value engineering components. Nevertheless, this is conflicted with the fact that compressive residual stress from AWJ cutting can restrain the crack initiation and growth while extending the fatigue life. Hence, it is worth to investigate the characteristics of AWJ cut workpiece surface and its influence on fatigue failure mechanism and compare these to other mechanical/-thermal machining processes (i.e. in this case with CFM, CRM and LAM). For this, abrasive waterjet machining is implemented in present research to cut a flat workpiece for the target fatigue specimen, as shown in Fig. 1 (c).

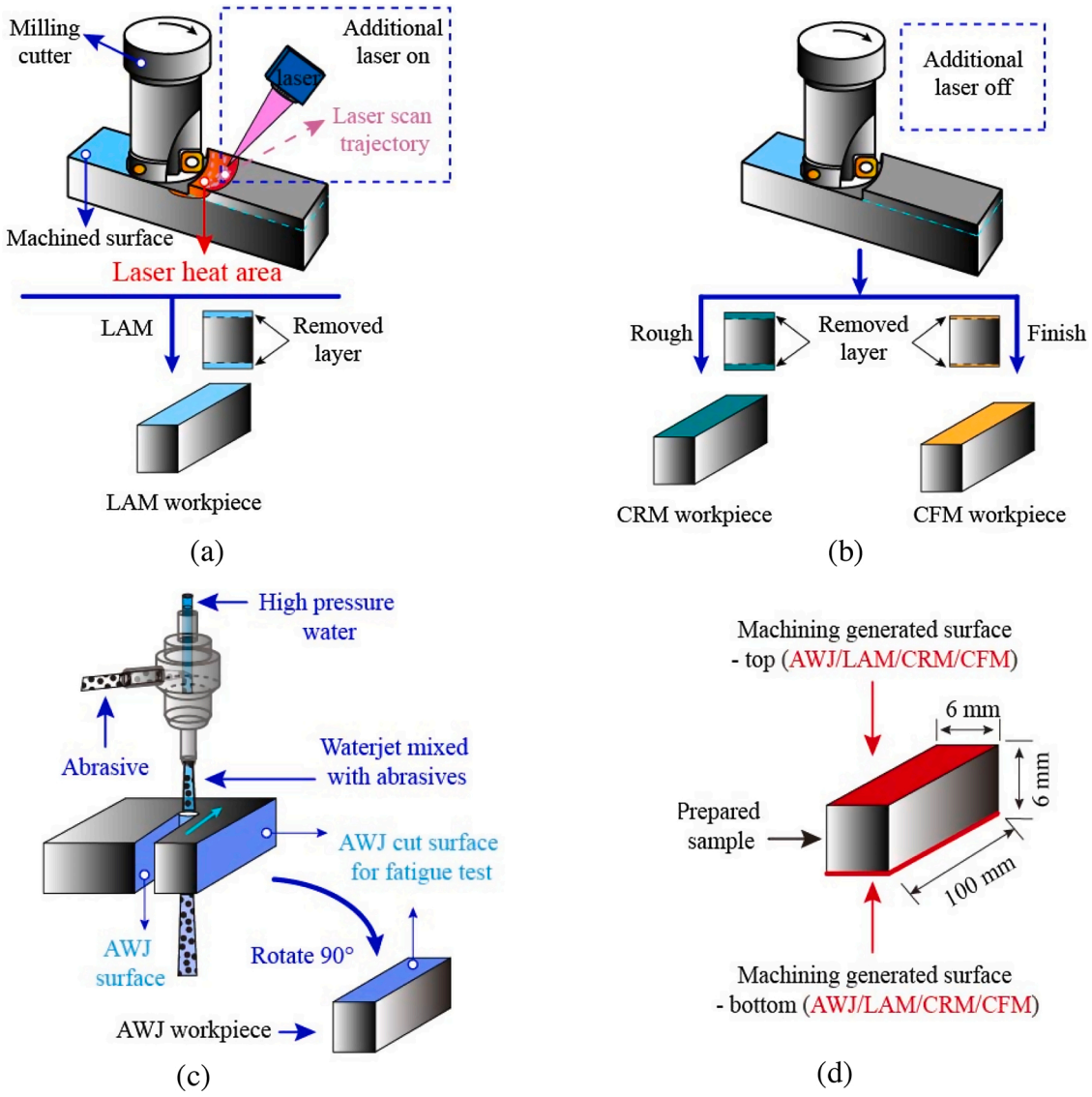

Fig. 1. Illustration of different cutting processes for generating samples for fatigue testing: (a) Laser assisted milling – LAM, (b) Conventional rough and finishing milling – CRM, CFM, (c) Abrasive waterjet cutting – AWJ, and (d) final workpiece employed for 4 points bending fatigue tests.

2.2. Specimen preparation

In the presented work, all specimens were cut from a single batch of Inconel 718 workpieces with the main chemical compositions and mechanical properties showing in Table 1, which was achieved through a solution anneal and age hardening heat treatment. That is, the material has been annealed at 980 °C and water cooled to room temperature, aged at 720 °C for 8 h, cooled with a rate of 56 °C/h to 621 °C and aged for another 8 h before cooled down with air. Small grain ageing state was reached with an average grain size of 15~30 μm after heat treatment, as shown in Fig. 2.

2.3. Experimental setup

All of the workpieces have been machined by the proposed conventional and non-conventional methods on both testing faces (see Fig. 1d) that will be loaded for four points bending fatigue test. The pre-optimised machining parameters adopted in present research can be found in Table 2. Apart from the two testing surfaces, all the other faces of the specimens were finish milled to reach a similar surface integrity while 0.5 mm radius chamfers have been introduced on the canners to eliminate the influence from the sharp edge stress concentration. In this paper, the AWJ cutting was implemented on a waterjet CNC machine (Waterjet AG; Fig. 3a) with an optimised pumping pressure of 400 MPa, jet feed speed of 30 mm/min and nozzle standoff distance of 0.5 mm.

Table 1
Chemical composition and mechanical properties of employed Inconel 718 superalloy.

	Cr	Ni	Mo	Co	Al	Ti	Nb	Fe	others
Chemical composition (%)	18.48	52.91	3.05	0.07	0.58	0.95	5.27	18.46	0.23
	Thermal conductivity (W/m°C)			Yield stress 0.2 % (MPa)		Young's modulus *E* (GPa)			Poisson's ratio *ν*
Mechanical properties	24 (900°C)			1250		212			0.294

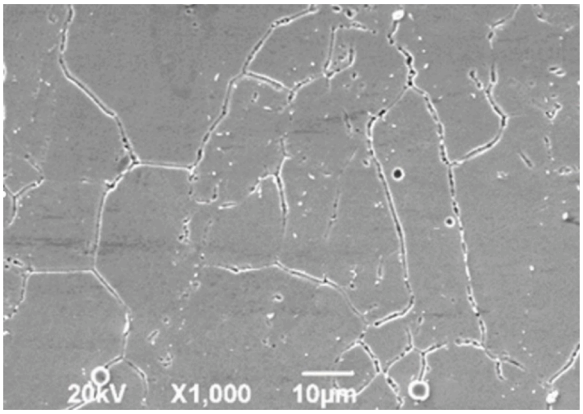

Fig. 2. Microstructure of the employed Inconel 718.

Table 2
Cutting parameters for different machining processes.

Methods	Depth of cut	Cutting width	Feed speed	Cutting speed	Laser power
LAM	0.25 mm	6 mm	0.25 mm/ tooth	45 m/min	1400 W
CRM	0.25 mm	6 mm	0.25 mm/ tooth	45 m/min	N/A
CFM	0.05 mm	6 mm	0.016 mm/ tooth	35 m/min	N/A

	Pump pressure	Jet feed speed	Abrasive	Abrasive flow rate
AWJ	400 MP	30 m/min	220 HPX BARTON	/min

Fine size garnet abrasives (220 HPX BARTON, mesh size of 170) were employed under 60 g/min abrasive flow rate. On the other hand, LAM test was implemented based on optimised laser scanning method (Shang et al., 2018) on a 5-axis milling machine tool with integrating a 10 kW diode continuous laser system (LDF mobile laser power made by LASERLINE Inc., scanning at a power of 1400 W and spot diameter 3 mm for this paper), as seen in Fig. 3(b). As to the conventional machining, both rough and finish milling processes were carried out on the same 5-axis machined tool without LAM system operating but under a flood coolant condition. A milling cutter (SECO-R217.21-3232.0-LP06.4A) with a diameter of 32 mm was used for LAM and conventional rough milling (CRM), while a solid carbide tool (SECO solid carbide JHP780060E2R030.3Z4-M64) was used for conventional finish milling (CFM) to remove the thermo-mechanical defects from CRM process. In order to eliminate the influence of tool wear, new inserts/tools were used for each cutting test.

2.4. Materials characterisation and fatigue testing

To investigate how the machining-induced thermal and mechanical loadings influence the machined surface integrity and further the fatigue failure mechanisms, both the surface topography and superficial layer metallurgical characteristics of machined workpieces were investigated at multiscale levels. The surface topography was revealed by Alicona G4 3D scanning system while the surface microstructure and cross-sections were prepared for microstructure analysis by using SEM (JEOL-6490) and EBSD (JEOL7100 F with Oxford Instrument), as well as the residual stress investigation by employing Proto iXRD.

To evaluate their fatigue performances and failure mechanisms, four points bending fatigue tests were conducted on the machined workpiece through a closed loop servo-hydraulic Instron testing machine (Fig. 4a). Sinusoidal loading cycles (stress ratio $\sigma_{min}/\sigma_{max} = 0.1$) at 5 Hz were run at room temperature in a constant loading mode, which produces a maximum stress on the loading surface of 80 %–140 % of the yield stress by applying corresponding parameters (Table 3) based on the bending relationship calculation outlined in Fig. 4(b) (Suárez et al., 2016). In this context, as shown in Fig. 4(b), the specimens, upon bending, deformed towards one fixed direction where the stress changed gradually from tensile to compressive condition from the bottom to upper face. The largest tensile stress appears at the bottom machined surface under bending deformation from which the fracture is expected to originate (Xu et al., 2018). To ensure statistically relevant results, the fatigue tests were conducted at least three times for each loading condition.

3. Surface integrity evaluation of workpiece machined from conventional and non-conventional processes

As mentioned before, nickel based superalloy is a difficult-to-cut material and extreme thermal/mechanical loadings can be imposed on the machined workpiece when conducting the conventional and non-conventional machining processes. This can eventually deteriorate the part surface integrity and so to influence the fatigue performance. Hence, to study the influence of machining induced surface alteration to the part fatigue performance, the surface integrity, including the surface topography, metallurgical and crystallographic modification as well as residual stress and nanohardness, will be investigated first in this section.

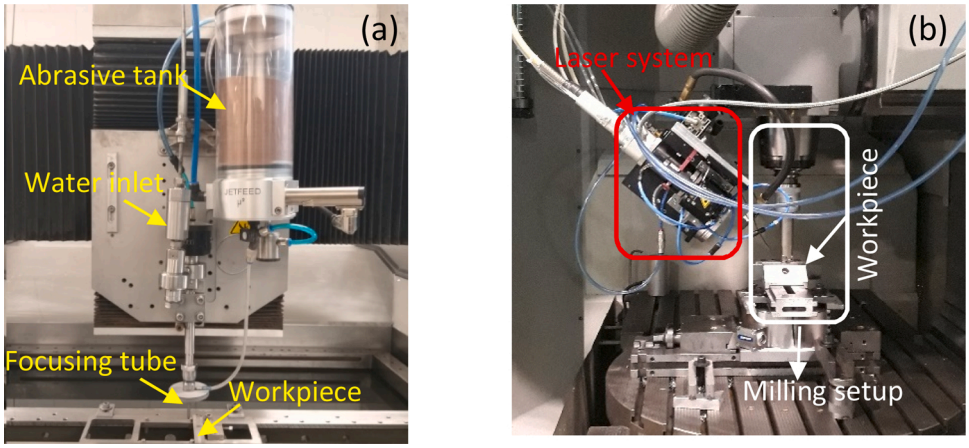

Fig. 3. Experimental setup for different machining processes: (a) Abrasive waterjet machining; (b) Laser assisted milling, Conventional rough and finishing milling (when laser switched-off).

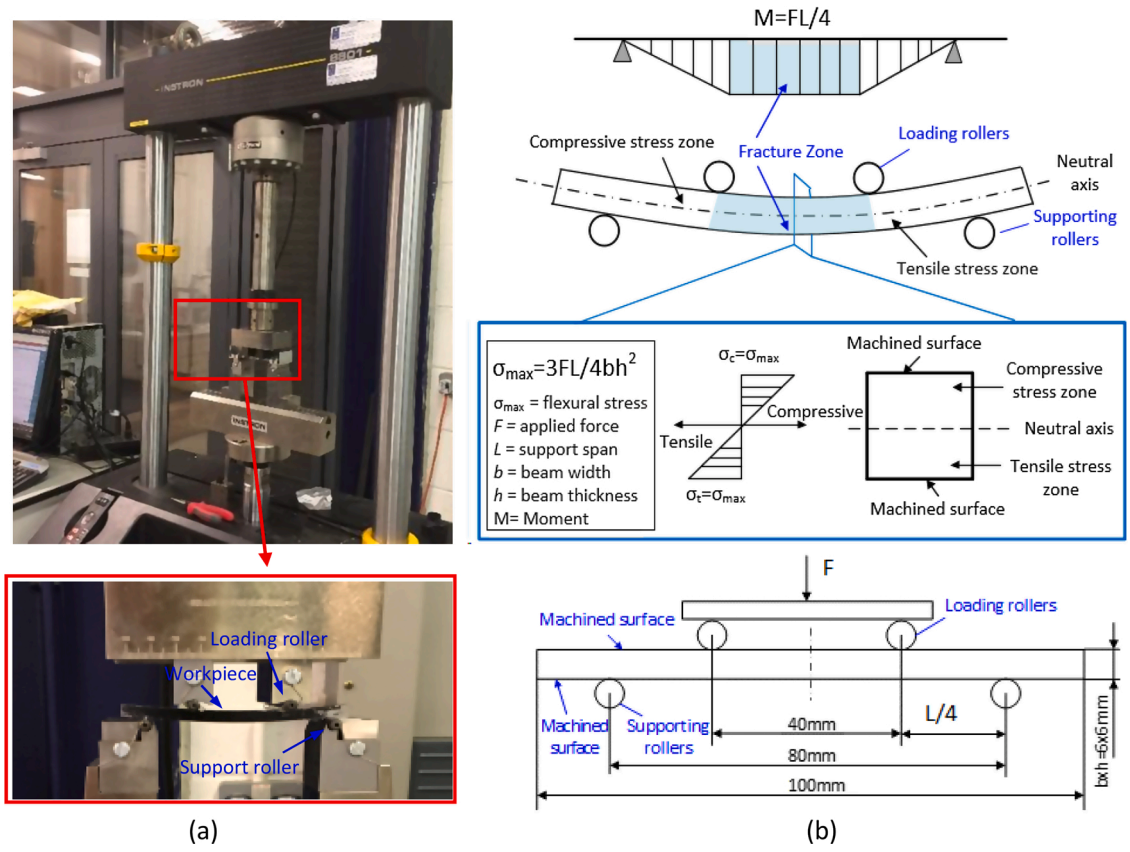

Fig. 4. Four points bending fatigue test: (a) experimental setup and (b) schematic illustration.

Table 3
Implemented fatigue test loading arrangement and setting.

Stress Level	80 %		100 %		120 %		140 %	
	Max	Min	Max	Min	Max	Min	Max	Min
Load thresholds (MPa)	1000	100	1250	125	1500	150	1750	175
Category	**AWJ**		**LAM**		**CRM**		**CFM**	
Total samples	12 samples		12 samples		12 samples		12 samples	

3.1. Surface topography

Surface topography, with which the formation of micro peaks and valleys may create localised stress concentration zones which can, at some extent, affect the fatigue strength. As the yielded surface roughness is naturally related to the material removal mechanisms, to investigate these machining effects, the surface topography from different machining methods has been measured on the machined workpieces, as shown in Fig. 5. The arithmetic mean value (Sa) and maximum height (Sz) are adopted to quantify the machined surface roughness (Fig. 6); thus, the observed features and differences can be traced back to the influence of the machining methods taken into consideration in this research. A higher surface roughness (both Sa and Sz) has been observed in CRM samples compared to the CFM one, while it is surprising that these values from CRM are comparable to the LAM milled surface although an improved machinability has been concluded with this process (Shang et al., 2019). This is because the surface roughness in milling process (CRM or LAM) is mainly determined by the trajectory of the cutting edges (dependent on feed per tooth and cutting edge radius), i.e. revolution marks, as shown in Fig. 5. It is also interesting to observe that although the abrasive waterjet cut (AWJ) workpiece shows a lower Sa (1.7 μm) than the milling process (1.8 μm of CFM, 3 μm of CRM and LAM), a much higher Sz has been achieved compared to all the milling process (87 μm of AWJ, 33 μm of CFM, 52 μm of CRM and LAM). This is because while there is no revolution machining marks in AWJ process (i.e. lower Sa) the abrasives impact induced local scratches can generate a large number of deep valleys on the workpiece surface, as indicated in Fig. 5(d), thus leads to a relatively higher maximum height (Sz) value. These valleys may increase the local stress concentration and further assist the initiation and propagation of the fatigue crack, namely micro-notch effect (Liao et al., 2019).

3.2. Surface microstructure

SEM observations of the microstructure on the machined surface (Fig. 7) can clearly indicate the geometrical and metallurgical damages of the machined surface. The CRM surface presents clear deep grooved milling marks (Fig. 7b) while these machining marks can be easily eliminated when employing finish milling process (Fig. 7a). Moreover, due to the aggressive cutting parameters in CRM process where high cutting forces and tool wear are yielded (Shang et al., 2019), micro-cracks can also be easily initiated when the cutting tool cuts through the precipitated carbides existent in the microstructure (Zhou et al., 2012). Moreover, some of these microcracks have also been observed propagating along the top surface (Fig. 7b), indicating a brittle feature of this layer, i.e. white layer which will be discussed later with cross section observation. Furthermore, surface tearing has also been observed on CRM sample which can be attributed to the dragging of particles (e.g. carbide or insert chipping) caused by the high cutting force. These micro defects can certainly influence the fatigue crack growth behaviour due to the local stress concentration and notch effect. Not surprisingly, material redeposition has been revealed on the LAM surface (Fig. 7c)

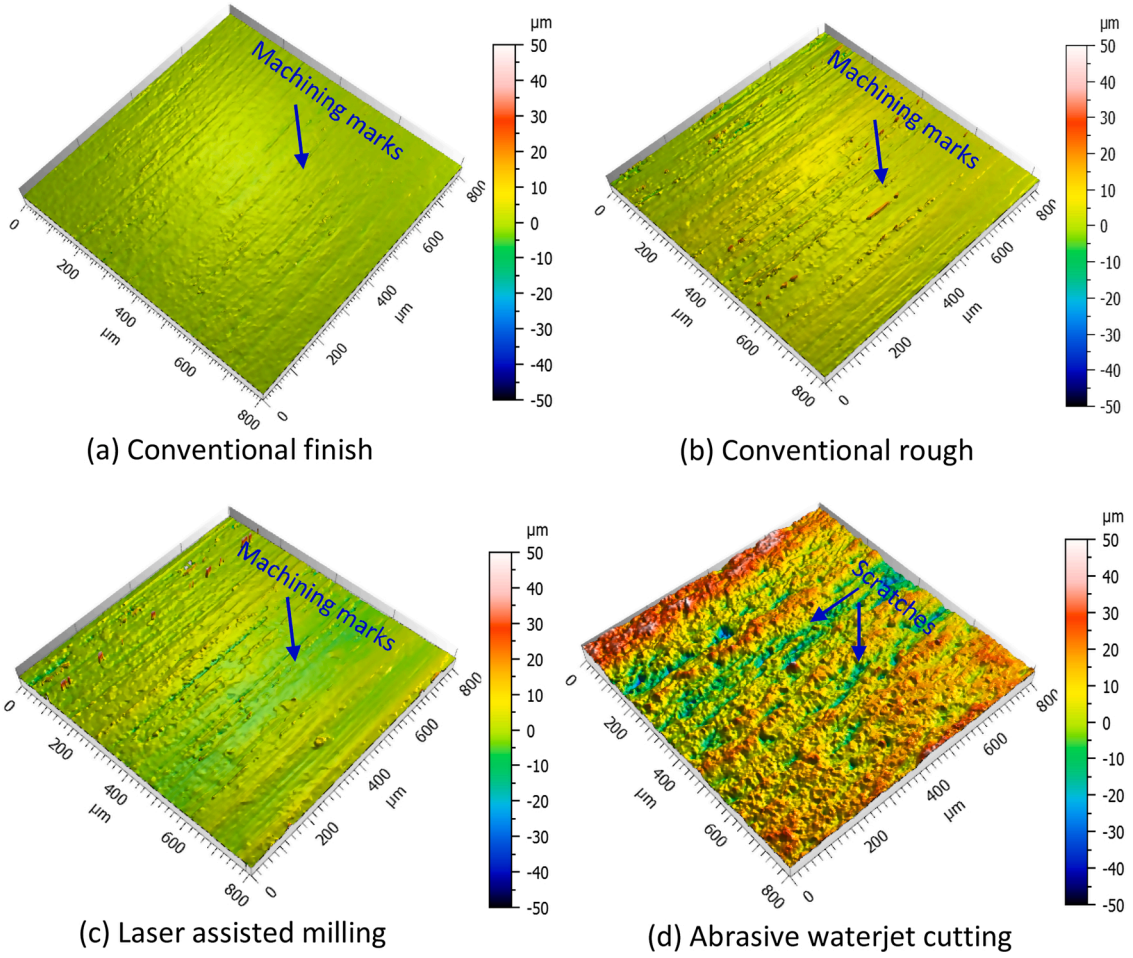

Fig. 5. Surface topography of workpiece machined by different processes: (a) Conventional finishing milling, (b) Conventional rough milling, (c) Laser assisted milling and (d) Abrasive waterjet cutting.

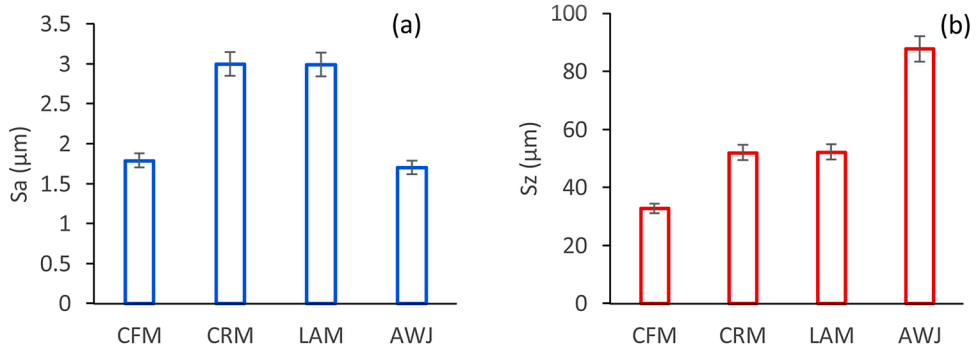

Fig. 6. Surface roughness of the machined surface: (a) arithmetic mean value - Sa, (b) maximum height - Sz.

which is caused by the adhesion of the molten workpiece material on the machined surface under high compression pressure and elevated temperature in LAM process. In the AWJ machined surface stochastically distributed scratches have been produced due to the impingement of high speed abrasive particles. Nevertheless, these hard abrasive particles can also be embedded into the surface/subsurface layer (Fig. 7d), which together with the scratches and chippings, can act as stress concentrators and initiate cracks during the fatigue test.

To investigate the mechanical and thermal effect on the microstructural characteristics of these machining methods, the cross section surfaces of corresponding surfaces are presented in Fig. 8. A thick white layer has been revealed on the CRM surface due to the high cutting temperature and mechanical strain. The white layer can significantly reduce the fatigue life of the nickel based superalloy parts due to its high brittleness whereby a crack can be easily initiated and developed in this layer, as shown in Fig. 8(b) (Chang et al., 2019). This layer, however, has been removed by the following finishing process as shown in Fig. 8(a) of CFM sample. It is interesting to observe that the LAM process generates a much thinner white layer although a high thermal energy has been introduced into this process. On the other hand, while a thick (~20 μm) material drag layer has been revealed in CRM process (Fig. 8b) due to the significant mechanical effect that deforms the grains in the superficial layer, this layer has been observed much thinner at LAM sample (~10 μm). This upgraded surface integrity can be attributed to the

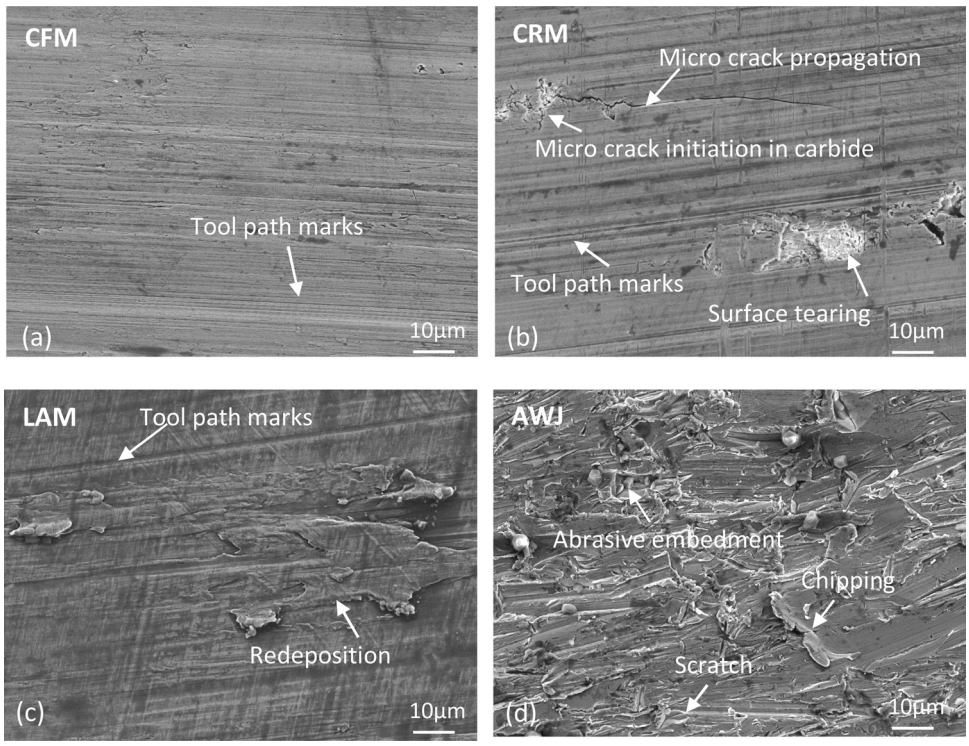

Fig. 7. SEM observation of machined surface microstructure: (a) CFM with grooved tool path marks, (b) CRM with grooved tool path marks, micro cracks and surface tearing, (c) LAM with grooved tool path marks and redeposition and (d) AWJ with abrasive embedment, chipping and scratches.

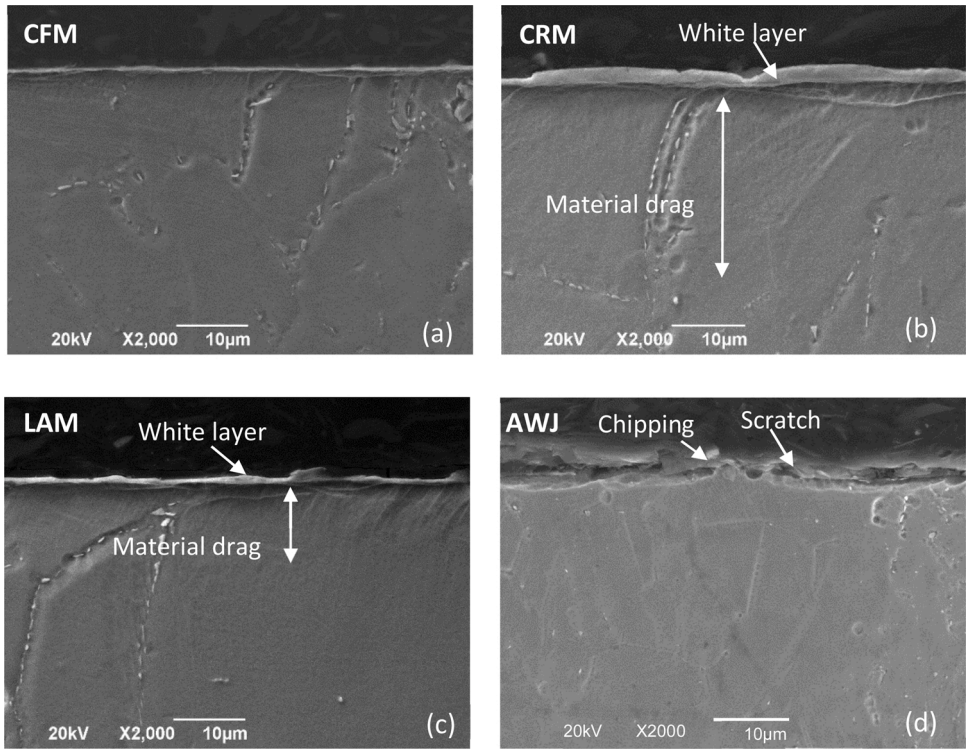

Fig. 8. Superficial surface microstructure SEM images of workpiece machined with different processing methods.

improved machinability of the thermally softened layer that was controlled under a certain depth and subsequently removed during the LAM process (Shang et al., 2019) whereby a gentler plastic deformation effect can be achieved accompanied by lower cutting force. Nevertheless, this plastic deformation layer has not been observed in pure mechanical process (i.e. abrasive waterjet cutting) but obvious scratches and chipping are presented (Fig. 8d).

The alteration of grain structures can also be clearly characterised by EBSD scanning, which can help understand how the thermal and mechanical loadings from the analysed machining processes change the

crystalline structure in the superficial layer, as shown in the inverse pole figure (IPF, Fig. 9a) and intragranular local misorientation (LMO) mapping (Fig. 9b). There is no clear recrystallisation detected in both the CRM and LAM surface due to the low indexing quality of ultrafine grains in white layer (Fig. 9a-ii and a-iii). However, a much smaller lattice deformation layer of LAM is observed compared to CRM samples that were machined with the same cutting parameters. This indicates the improved machinability and surface integrity of LAM due to controlled-depth thermal softening of the workpiece material, which is consistent with above observations of grain deformation (Fig. 8b and c). It is also interesting to observe that the mechanically induced lattice deformation from waterjet cutting (Fig. 9b-iv) is even higher than conventional finish milling (Fig. 9b-i) although the metallurgical observation on the cross section shows no deformed grains (Fig. 8d). This can be attributed to the high density micro defects (e.g. scratches and abrasive embedment, Fig. 8d) which can generate localised stress concentration on the superficial layer although no grain deformation has been produced due to the low cutting force.

To further understand the extent of plastic strain in the machined superficial layer, the average intragranular misorientation (AMIS) (Brewer et al., 2006) is employed for quantifying the lattice deformation. As shown in Fig. 10, the extent of surface plastic strain is indicated by the AMIS profiles as a function of depth from the machined surface, whereby a high AMIS near the machined surface has been revealed under all cutting methods due to the plastic deformations while with the increased distance from the surface its value drastically reduces. Along these, LAM shows the highest plastic strain on the superficial layer indicating a most severe lattice deformation due to the externally induced thermal effect combined with the machining induced mechanical effect in the material. On the other hand, CRM demonstrates a largest depth (~30 μm) of high value AMIS, which coincides with the metallurgical observation of the cross section (Fig. 8). Interestingly, although AWJ process yields low cutting forces, a 5 μm depth of high value AMIS has been observed, which can be attributed to the high extent of localised deformations caused by the high speed abrasive particles impinging on the workpiece surface.

Microstructural defects (e.g. white layer, grain deformation), as factors that can facilitate the crack initiation and propagation, can significantly reduce the fatigue life (Herbert et al., 2014) as mentioned before. However, except the surface defects, the fatigue performance of the machined workpieces could also be influenced by their mechanical characteristics (e.g. residual stress and hardness) under different mechanisms. Hence, although an improved surface integrity has been observed in LAM process, it is not clear if its fatigue performance would be improved before the workpiece inherent stress condition is known.

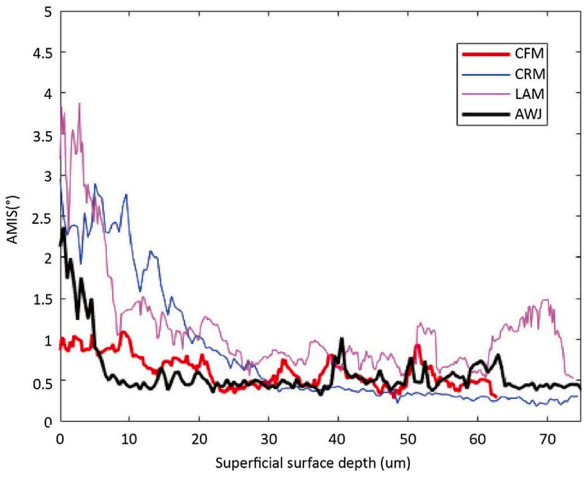

Fig. 10. Average intragranular misorientation (AMIS) profile as a function of depth under the free surfaces generated by different machining methods.

Thus, a further investigation of the residual stress and nanohardness will be conducted in the following section to understand the mechanical property alterations of the machined surface.

3.3. Residual stresses and hardness

Naturally, the subsurface residual stress profile (Fig. 11) of machined workpiece from XRD measurement have been provided to present the stress conditions residual in the workpiece after machining. It is obvious that the LAM workpiece (Fig. 11a) shows the highest tensile stress on the top surface while a unique stress distribution (i.e. high tensile stresses appear again at the depth of around 300 μm) is found in the subsurface area. This phenomenon can be attributed to the significantly higher level of thermal energy induced by the laser heating that penetrates much deeper into the workpiece when compared to the pure milling process, which results in a tensile stress condition even in the deeper zones (300 μm) below the top workpiece surface (Xu et al., 2020a). On the other hand, the mechanical effect partition from cutting tool engagement on the surface layer (at the depth of 100 μm) reduces the tensile stress level by compensating with compressive stress while this mechanical effect disappears at a deeper layer (i.e. 300 μm) hence leading to a wavy shape. As comparison, both the conventional finish milling (CFM) and abrasive waterjet (AWJ) cutting processes generate slight level of compressive residual stresses in both surface and subsurface zones. While the AWJ workpiece presents the largest compressive residual stress at the surface

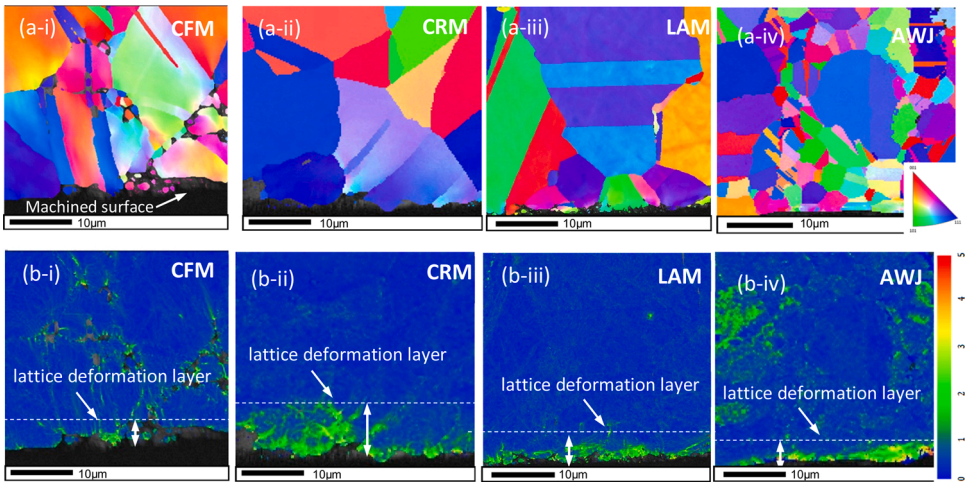

Fig. 9. IPF (a) and LMO (b) from EBSD scanning revealing the superficial crystalline microstructure of workpiece machined with different methods.

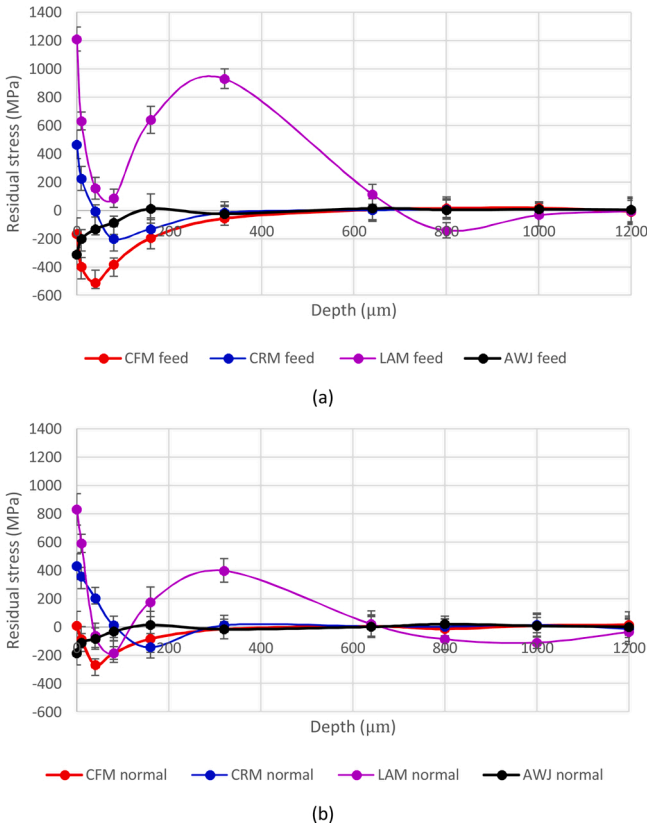

Fig. 11. Residual stress profile in the superficial surface layers of workpieces machined with different techniques in both feed (a) and normal (b) directions.

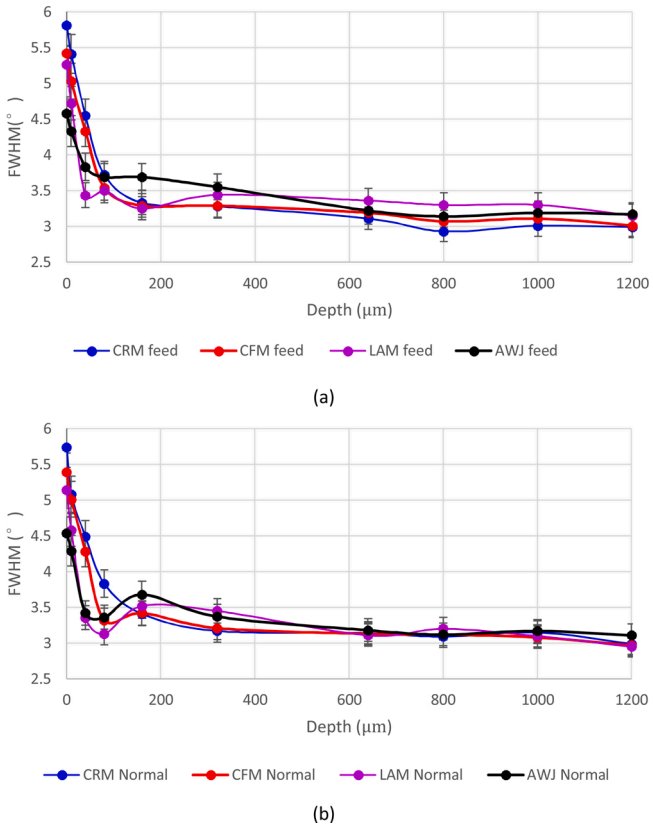

Fig. 12. FWHM profile in superficial surface areas of machined workpiece with different techniques at both feed direction (a) and normal direction (b).

area (−311 MPa) caused by the mechanical impacts of the abrasives, the largest compressive residual stress (−510 MPa) in CFM sample appears at the depth of around 40 μm (Fig. 11a) as a result of the combined thermal and mechanical effect (Liao et al., 2021). As expected, the conventional rough milling (CRM) samples show a similar distribution trend with the CFM ones, while the values are larger which is because the rough milling process, with high values of the cutting parameters, produces more heat which leads to higher levels of tensile stress (465 MPa at the surface area). In addition, the residual stress distribution in normal direction (Fig. 11b) displays the same tendencies/patterns with the one described in the feed direction Fig. 11(a). Naturally, as the tensile stress can facilitate the initiation and propagation of fatigue cracks and surface rupture, the LAM samples are foreseen to have the shortest fatigue life.

Further, the corresponding full width at half maximum (FWHM, Fig. 12) of X-ray diffraction peak is employed to indicate the micro-structural changes (e.g. plastic strain) in the superficial layers after machining (Li et al., 2009). A highest FWHM value (5.8°) is found at the surface for the CRM samples and then rapidly decrease to bulk state (~3°) at around 200 μm (Fig. 12a), while the CFM samples show slightly smaller values with the same trend. The peak width broadening (larger values on top surface) for both CRM and CFM samples are attributed to the plastic deformation induced by the cutting tool engagement during the processes. Interestingly, as contrast, the FWHM of LAM sample shows a lower broadening effect (i.e. smaller value) and quicker decrease in the depth direction, which is attributed to the thermal softening effect that lower cutting force/ mechanical deformation (Shang et al., 2019) and higher thermal expansion are yielded during this process. These observations have shown a good correlation with the results presenting subsurface microstructural characteristics, whereby the CFM process produces the best surface integrity while the CRM samples generate the largest subsurface alternation and the LAM samples show less deformation but significant tensile stress compared to CRM. As regards to the AWJ samples, which have only been influenced by the localised abrasive impacts, they show the smallest half peak width value at the surface comparing with the milling processes (CFM, CRM and LAM), indicating a smallest broadening effect, i.e. plastic deformation, due to low cutting force involved in this process.

To characterise the subsurface mechanical properties, nanohardness-depth profiles (Fig. 13) have been acquired by employing indentations on all samples with Berkovich tips (loading control - 25 mN) with five times repetition at each case. Interestingly, it is found that the hardness of samples acquired from both LAM and CRM processes demonstrate a significant softening phenomenon. That is, the hardness for LAM sample is 3.28 GPa at the near surface area (~3 μm) and 4.62 GPa for CRM samples, values which are significantly lower when compared to the bulk state (7.0 GPa). While this softening effect is induced by the

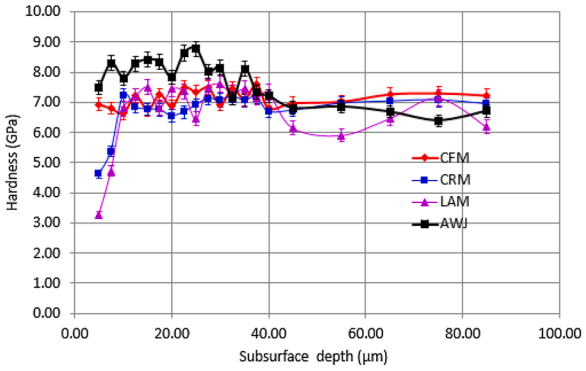

Fig. 13. Hardness profile of machined different workpiece in superficial surface areas.

thermal influence (either machining generated heat and/or externally introduced laser heat), the pure mechanical loading in AWJ machining (i.e. high speed abrasive impingement) leads to obvious work hardening effect on the superficial layer (i.e. > 8 GPa until the depth of 30 μm beneath machined surface). As to the CFM machined workpiece, no noticeable hardness variation is found in the superficial layer due to the low cutting force and temperature. These observations indicate that the metallurgical surface integrity can only partially reflect the materials alteration, hence further mechanical measurement (e.g. residual stress and hardness) are required for in-depth understanding the influence of machining to component functional performance, e.g. fatigue failure mechanism.

4. Fatigue performance

4.1. Fatigue life and fractography

Fig. 14 shows the fatigue life distributions as a function of applied stress amplitude for the samples machined by the routes presented before. As seen from the comparison of experimental S-N curve, the CFM samples present the longest fatigue life resulted from its preeminent surface integrity. Compared to CFM machining, the fatigue life of AWJ cut samples is naturally shorter due to the high density of scratches and abrasive embedment that deteriorate the surface condition, i.e. localised stress concentration. On the other hand, the fatigue life of AWJ cut samples is also obviously longer than CRM/LAM ones because of its surface hardening effect, e.g. compressive residual stress and elevated hardness on the superficial layer of AWJ samples, as presented in Figs. 11 and 13. As the thermally induced tensile residual stresses in the workpiece superficial layer can facilitate the initiation and propagation of fatigue cracks, as mentioned in Section 3.3, the LAM samples have presented the shortest fatigue life. However, it is surprise that this only occurs in high cycle fatigue (HCF) while in low cycle regime (i.e. maximum stress > 100 % yield stress level) it shows a slightly longer fatigue life compared with CRM samples. This indicates that when the maximum loading stress is below the yield stress, i.e. caused by elastic deformation in each cycle, the residual stresses play an important role in determining the fatigue life while when the maximum stress is above the yield stress (i.e. low cycle fatigue) the fatigue life is mainly influenced by the metallurgical surface defects (e.g. white layer and grain deformation). This is because at low cycle fatigue (LCF) the plastic deformation occurs in each cycle and leads to the rapid stress relaxation at the early stages of fatigue cycling (Aigner et al., 2019; Novovic et al., 2004), in which scenario mainly the surface defects influence the fatigue performance with dominating its crack initiation and propagation. Table 4 lists the combination of fatigue life and the influence of each factor of surface integrity. However, it should be noted that the effect of surface integrity to fatigue life is a complex combination of different factors that needs to be judged based on specific cases as mentioned above.

SEM and optic microscope observations have allowed the fractography analysis of fatigued samples under various magnifications to reveal their fracture mechanisms in different surface integrity states. The general characteristics of Inconel 718 fractured surface can be categorised into two different areas, namely fatigue induced and static breakage areas (Fig. 15) (Belan et al., 2018). The fatigue induced fracture area demonstrates a brighter contrast in optic micrograph (Fig. 15a) as the fracture surface appears mainly with cleavage plan features (Fig. 15c) which is more reflective. These cleavage ruptures can be associated with brittle fracture that is dominated by cleaving of the crystals along crystallographic planes (transgranular) or grain boundaries (intergranular) (Lu et al., 2020), namely brittle fracture area. On the contrary, the static breakage appears in compressive stress side, which represents the mechanism of ductile transcrystalline fracture associated with dimple patterns (Fig. 15b), namely ductile fracture area. A transition zone is also observed in between these two areas wherein a mixed of cleavage features and dimples, which are accompanied with secondary cracks, are distinguished (Fig. 15d).

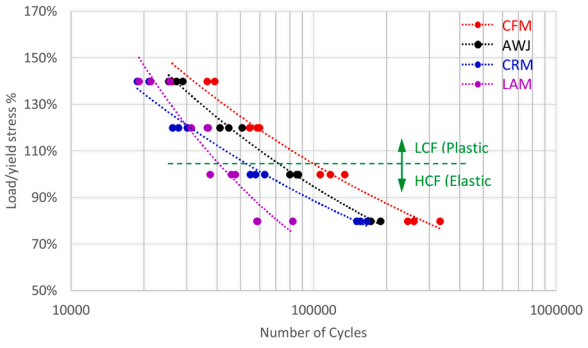

Fig. 14. Fatigue life results comparison of workpiece machined from different processes.

More specifically, in fatigue fracture area the crack normally grows from the deflected region, e.g. misoriented grain boundary of two conjunct grains (intergranular mode) and propagates along the favoured slip planes in γ matrix (Gao et al., 2007) (transgranular mode) with a relatively low propagation rate, whereby a cleavage plane is generated (normally along {111} planes for nickel-based superalloy (Mills and Brown, 2001)), as shown in Fig. 16(a) and (b). While these cleavage remains in large planes, the stair-step featured fracture can also occur adjacent to the grain boundary, i.e., cleavage steps, as shown in Fig. 16 (a) and (b), via a transgranular mode. This mainly occurs in the brittle fracture area accompanied with a plastic deformation in adjacent grains, where the multiple slip systems must act in concert to maintain continuity between grains (Mills and Brown, 2001). With the increasing distance from the machined surface, the crack propagation rate increases and ductile fatigue striations are generally dominant, associated with a ductile growth mechanism. When reaching the transition area, a combination of ductile fatigue striations and dimples dominates the fracture propagation while secondary cracks also occur due to the restriction of carbide inclusions (Fig. 16c). Finally, in static fracture area the main fracture presents a large number of dimple ruptures which are associated with plastic deformations mechanism, as shown in Fig. 16(d), indicating a much higher crack propagation rate compared with fatigue fracture area. These observations compose the main crack propagation mechanisms of the tested material while their characteristics can also be influenced by the different machined surface integrity, which will be discussed in the following investigations associated with specific machined samples.

4.2. Crack initiation and propagation of fatigue samples under different machining methods

When looking into the crack initiation and propagation areas under different machining methods, similar geometries of propagation marks were generally observed in these fatigue samples (Fig. 17). Specifically, while the fracture propagation marks present a sectorial shape, many ridges are also observed extending in the radial direction, i.e. the crack growth path. The higher magnification SEM observation shows that the crack initiation sites present varied morphologies for these four machined surfaces, which, combined with the previous surface integrity investigation, can allow the in-depth understanding of fatigue crack initiation mechanisms that influenced by different machining methods. Interestingly, while all the other samples show a crack initiation from the machined surface (Fig. 17b–d), the CFM sample (Fig. 17a) presents a crack initiation site from the chamfered corner. This is, possibly, because of the high surface integrity of the CFM samples (Table 4) with which it is difficult to nucleate a crack site on the machined surface, hence the crack initiates from the stress concentration area, i.e. corner of the sample. The CRM and LAM samples show a single crack initiation source located on the machined surface with a small fan-shaped area (Fig. 17b

Table 4
Critical evaluation of the influence of surface integrity upon fatigue life.

	CFM	AWJ	CRM	LAM
Fatigue life (Maximum cycles)	Long (330000)	Medium (188000)	Short (160000)	Very short (81000)
Surface topography (Sz)	Very good (32 μm)	Poor (87 μm)	Fair (52 μm)	Fair (52 μm)
Metallurgical alteration (deformation layer)	Very good (1 μm)	Very good (0 μm)	Poor (20 μm)	Fair (10 μm)
Crystallographic alteration (LMO depth)	Very good (5 μm)	Fair (10 μm)	Poor (20 μm)	Fair (10 μm)
Residual stress (On surface)	Very good (-200 MPa)	Very good (-311 MPa)	Fair (465 MPa)	Poor (1210 MPa)
Hardness (On surface)	Good (6.9 GPa)	Very good (7.6 GPa)	Fair (4.6 GPa)	Poor (3.2 GPa)

Note: **Red** and **Green** colour indicate positive influence to the fatigue life, while **Blue** and **Grey** colour indicate medium and negative influences respectively

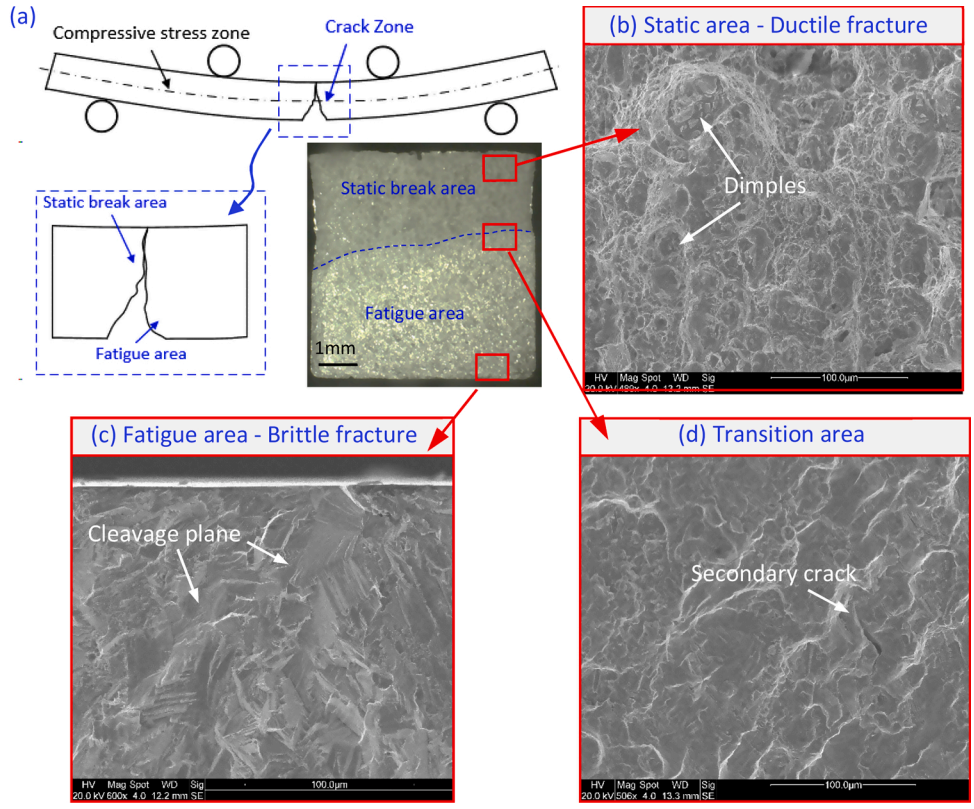

Fig. 15. Overall view on fractured surface: (a) overview of fracture morphology, (b) static breakage, (c) fatigue induced and (d) transition areas.

and c). On the contrary, the waterjet fractured sample appears as a conjunction of multiple crack initiation sites on the machined surface. This is namely in line with the surface damages in waterjet machining process whereby large number of scratches and abrasive embedment have been generated (Fig. 7d) that can initiate the crack during the fatigue test. On the other hand, the crack initiation site in AWJ sample is smaller as it is initiated from the stress concentration area (e.g. scratch or abrasive embedment) while the milled samples (e.g. CRM and LAM) have much bigger crack initiation features as they are initiated from the metallurgical defects (e.g. white layer and material drag - Fig. 8) which are associated with lager dimensional damages and material properties alteration (e.g. hardness - Fig. 11 and residual stress - Fig. 13).

A closer observation at the machined subsurface reveals the crack growth morphology on fatigue area which demonstrates a close relation to the surface defects induced by different machining processes. It is apparent that the feature of cleavage rupture dominates the crack growth area of all these four scenarios (Fig. 18), i.e. crack growth along the favoured crystallographic slip planes or grain boundaries. The conventional finish milled (CFM) sample reveals a higher density of fatigue striation marks beneath the machined surface indicating a lower crack growth rate (Mills and Brown, 2001) resulting from the compressive stresses (Fig. 11) and high metallurgical surface integrity (Fig. 8). A skinning zone in conjunction with the cleavage steps has been observed specifically in the conventional rough milled (CRM) sample which can be correlated with the machining induced white layer and grain deformation respectively (Fig. 18b). This demonstrates that the crack incrementally emanates along the slip band formed in the deformed grains (i.e. material drag) beneath the machined surface while the white layer

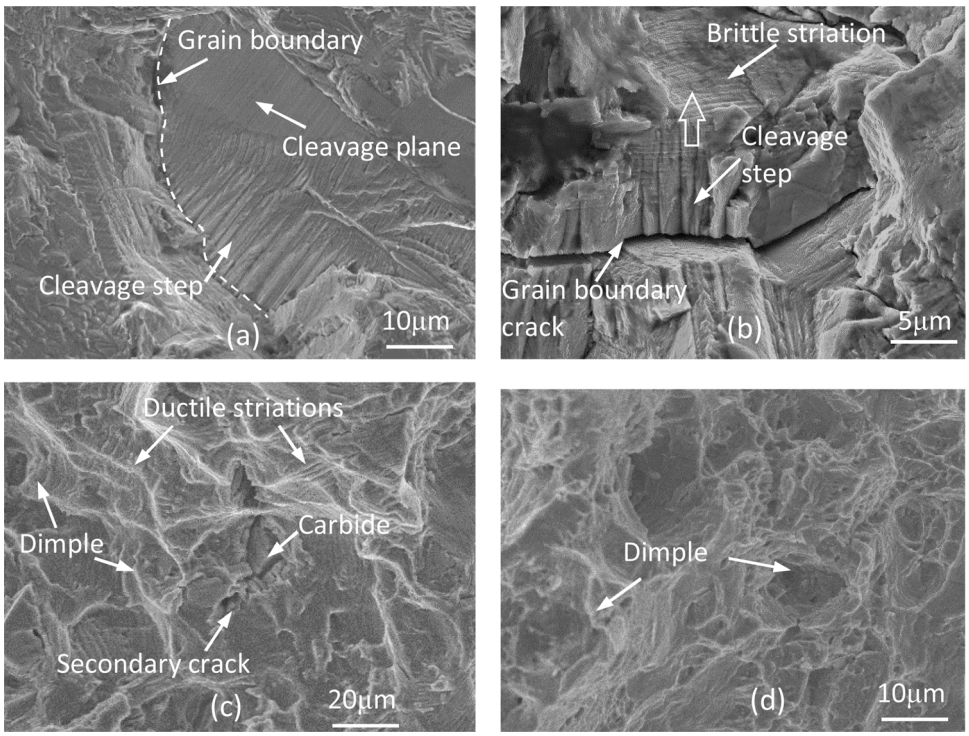

Fig. 16. Examples of common morphologies on the fracture surface of Inconel 718 under four points bending fatigue testing: (a) and (b) fatigue crack area, (c) transition area and (d) static crack area.

forms a skinning zone due to the small grain size of this layer that stops the cleavage growth grain. When it comes to the LAM sample a similar skinning zone has been observed in the machined surface while however it is much thicker (10 μm) than the CRM one (3 μm). This skinning effect namely forms in the severely heat affected/softened layer where the material underwent over-aging and can be peeled off from the machining induced compressed layer (i.e. deformed grains). As a crammed series of narrow scratch traces originating at the AWJ machined surface (Fig. 7d), a number of cleavage steps were produced beneath the scratched area where the materials have been plastically deformed/strengthened that restrains the cleavage growth hence forms the stair-steps. High density fatigue striations were also observed in AWJ samples due to the positive action of compressive residual stress.

While the brittle fatigue striations in the fatigue fracture area are generated through the alternating blunting and resharpening of the crack tip during each loading cycle (Mills and Brown, 2001), this phenomenon can also be influenced by the metallurgical alteration of the superficial layer, i.e. surface integrity. Hence, to quantitatively study the fatigue crack propagation of those samples from different machining processes, the fatigue striations, which demonstrates the magnitude of the fatigue deformation/strain, have been investigated on the fracture surface at the same distance of 50 μm from the crack initiation sites. In this scenario, the fatigue striations from the brittle fracture area not only highlight the direction of primary fatigue crack propagation in these specimens, but also indicate the crack propagation rates through the quantified striation spacing per cycle (D), as shown in Fig. 19. While the conventional finish milled (CFM) specimen presents the smallest striation spacing (0.22 μm/cycle, Fig. 19a), the LAM specimen demonstrates a larger value (0.34 μm/cycle, Fig. 19c). This is attributed to the high thermal influence on the LAM process whereby a high tensile residual stress figure leads to a higher crack propagation rate. Nevertheless, due to the positive action of residual compressive stress in the machined superficial layer (Fig. 11), the AWJ cut specimen presents a similar striation spacing (0.24 μm/cycle, Fig. 19d) with that of the conventional finish milled (CFM) specimens, while a slightly larger striation spacing is observed in rough milled specimen (0.28 μm/cycle, Fig. 19b) which can be associated with a tensile residual stress from machining effect. These observations demonstrate that the machining induced mechanical effects can retard crack propagation rates (e.g. mechanically induced compressive stress) while the thermal effect can accelerate the crack propagation rates (e.g. thermally induced tensile stress).

5. Conclusion

While fatigue performance of nickel based superalloy is of high importance for its application in safety critical applications, understanding the influence of machining induced surface integrity on fatigue failure and the mechanisms leading to this fracture/failure from these machining generated characteristic represents a crucial aspect for rational understanding of the superalloy machining. This paper studies the influences of mechanical and thermal loadings induced by different machining processes, i.e. conventional finish (CFM) and rough milling (CRM), laser assisted milling (LAM) and abrasive waterjet cutting (AWJ), upon the fatigue performance of nickel based superalloy. In-depth surface topographical and metallurgical investigations on the machined surface have been conducted and validated with four points bending fatigue test as well as fractography analysis. It is shown that CFM yields the best surface integrity with including topographical, metallurgical and mechanical aspects due to the low cutting force/temperature and eventually longest fatigue life. AWJ samples rank the second long fatigue life although high density of surface scratches and abrasive embedment has been found. Due to the high cutting temperature introduced by the internal cutting energy (i.e. CRM) or externally heat source (i.e. LAM) a white layer and deformed grains have been demonstrated accompanied with high tensile residual stress and softening effect on the machined superficial layer and yield a complicated fatigue performance. The main findings of the paper can be summarised as follows:

1 An obvious higher fatigue life is observed in CFM compared with CRM process indicates a final finishing process can eliminate the both the surface defects and tensile residual stress from roughing

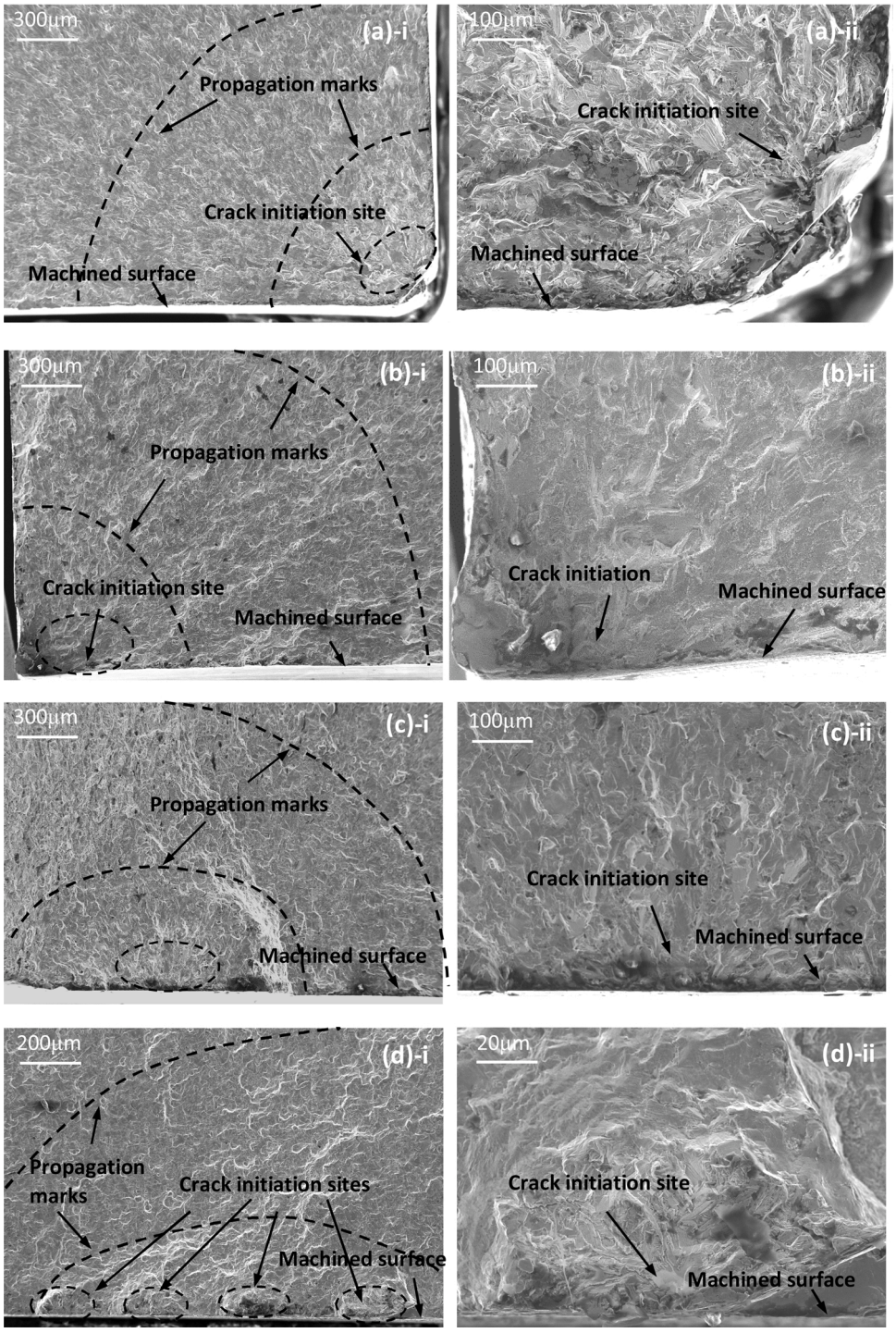

Fig. 17. Crack initiation and propagation in the machined surface with different magnifications: (a) conventional finish milling (CFM), (b) conventional rough milling (CRM), (c) laser assisted machining (LAM), (d) abrasive waterjet cutting (AWJ). All images are collected from the fractured samples under 1250 MPa maximum loading stress.

process. AWJ machined surface, although has been hardened by the abrasives' impact, this yields shorter fatigue life than CFM samples due to the high-density local stress concentrators (e.g. scratches and abrasive embedment).

2 While LAM workpiece shows a similar surface topography and less metallurgical damage compared with the CRM process, the fatigue life is however shorter than that of CRM in HCF regime due to the higher tensile residual stress. Nevertheless, when the maximum loading stress exceeds yield stress (i.e. LCF) the fatigue performance is dominated by the metallurgical surface defects that longer fatigue life has been achieved by LAM sample.

3 The formation mechanism of crack initiation site is naturally determined by the surface defects whereby a single crack initiation source from the machined surface appears on the CRM and LAM samples while the AWJ sample demonstrates a conjunction of multiple crack initiation sites due to the high density stress concentrators.

4 While the CFM and AWJ samples reveal a higher density of fatigue striation marks beneath the machined surface the CRM and LAM

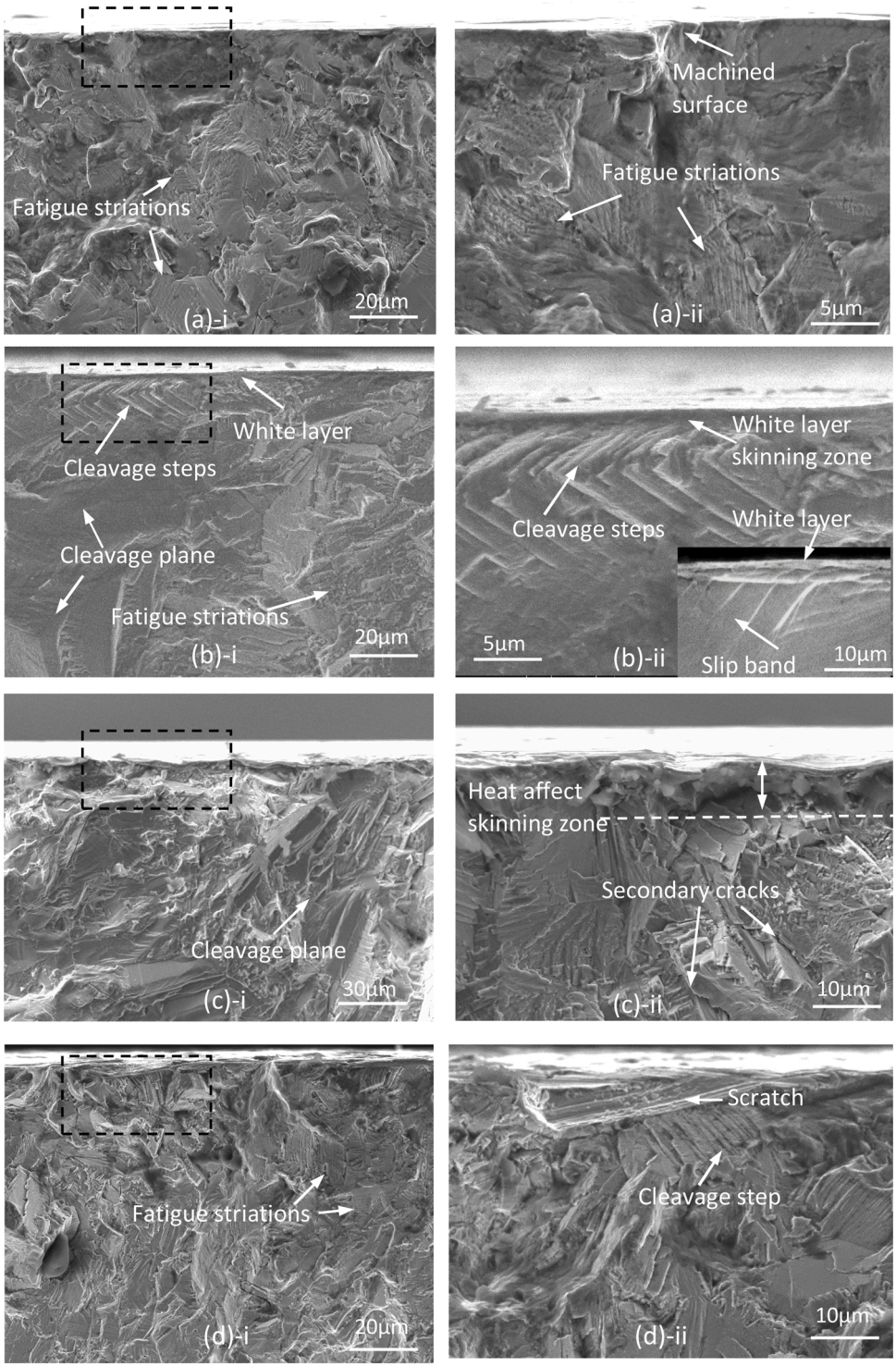

Fig. 18. Crack growth morphology on the machined subsurface: (a) conventional finish milling, (b) conventional rough milling, (c) laser assisted machining, (d) abrasive waterjet cutting. All images are collected from the fractured samples under 1250 MPa maximum loading stress.

samples demonstrate a skinning zone due to the small grain size of white layer/overaged layer that stops the cleavage growth. A number of cleavage steps have also been produced beneath the scratched area of AWJ sample due to the localised plastic deformation that restrains the cleavage growth.

5 From the fatigue life observation it can be generally concluded that the machining induced residual stress can significantly affect the fatigue life in HCF regime dominated by elastic deformation, while this influence is not obvious in LCF regime as the stress can be released at the early stages of fatigue cycling under plastic deformation that occurs in this regime. On the other hand, the crack initiation and propagation morphology indicate that the topographical and metallurgical alterations of the machined surface can crucially contribute to the crack initiation and fracture propagation mechanisms under fatigue loading.

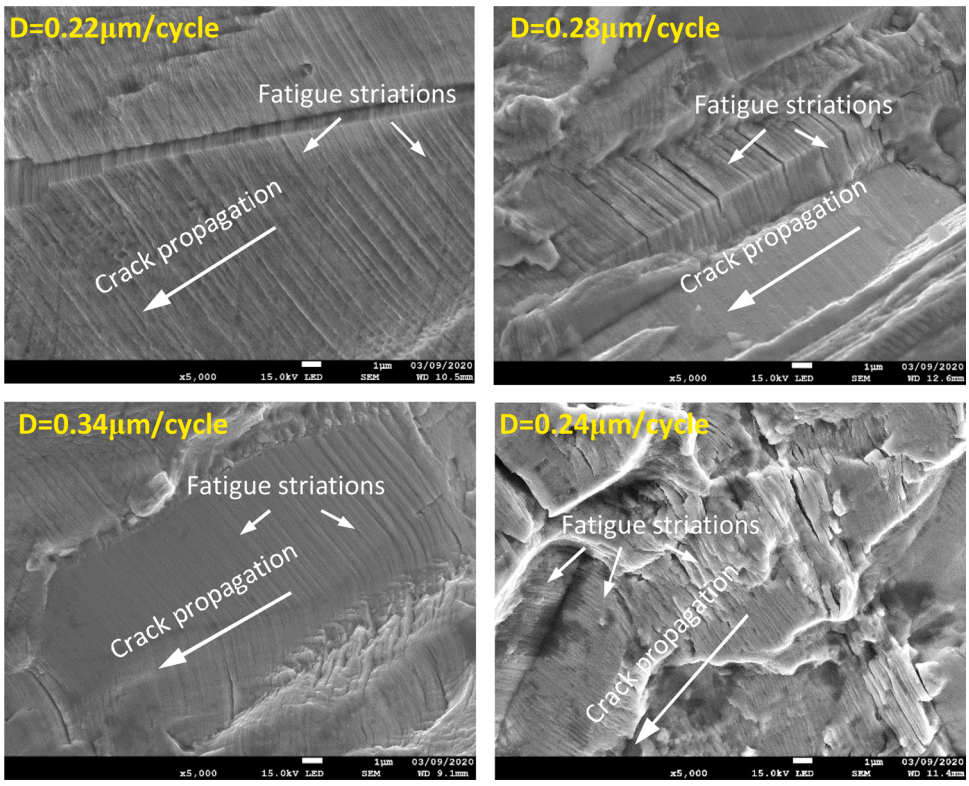

Fig. 19. Brittle fatigue striations on the fatigue crack area: Conventional finish milling, (b) Conventional rough milling, (c) laser-assisted machining, (d) abrasive waterjet cutting. All images are collected from the fractured samples under 1250 MPa maximum loading stress.

CRediT authorship contribution statement

Zhirong Liao: Conceptualization; Methodology; Experiment; Investigation; Writing- Original draft preparation; Project management. **Dongdong Xu**: Conceptualization; Methodology; Experiment; Investigation; Review and Editing. **Dragos Axinte**: Conceptualization; Supervision; Funding acquisition, Review and Editing. **Gonzalo García:** Investigation; Review & Editing. **Giedrius Augustinavicius:** Experiment; Review & Editing. **Jon Ander Sarasua**: Experiment; Review & Editing. **Anders Wretland**: Funding acquisition, Review and Editing.

Declaration of Competing Interest

The authors declare that they have no known competing financial interests or personal relationships that could have appeared to influence the work reported in this paper.

Acknowledgements

This project has received funding from the Clean Sky 2 Joint Undertaking under the European Union's Horizon 2020 research and innovation programme under grant agreement No. 754807. This study was also supported by EPSRC through NanoPrime (No: EP/ R025282/1). Our partners GKN Aerospace Sweden AB and SECO Tools AB are also acknowledged. The authors thank the support from Nottingham research fellowship programme as well.

References

Aigner, R., Pusterhofer, S., Pomberger, S., Leitner, M., Stoschka, M., 2019. A probabilistic Kitagawa-Takahashi diagram for fatigue strength assessment of cast aluminium alloys. Mater. Sci. Eng. A 745, 326–334. https://doi.org/10.1016/j.msea.2018.12.108.

Belan, J., Vaško, A., Kuchariková, L., Tillová, E., 2018. The fractography analysis of IN718 alloy after three-point flexure fatigue test. MATEC Web of Conferences 157. https://doi.org/10.1051/matecconf/201815707001.

Brewer, L.N., Othon, M.A., Gao, Y., Hazel, B.T., Buttrill, W.H., Zhong, Z., 2006. Comparison of diffraction methods for measurement of surface damage in superalloys. J. Mater. Res. 21 (7), 1775–1781. https://doi.org/10.1557/jmr.2006.0199.

Chaabani, S., Arrazola, P.J., Ayed, Y., Madariaga, A., Tidu, A., Germain, G., 2020. Comparison between cryogenic coolants effect on tool wear and surface integrity in finishing turning of Inconel 718. J. Mater. Process. Technol. 285 https://doi.org/10.1016/j.jmatprotec.2020.116780.

Chang, L., Volpe, L., Wang, Y.L., Burke, M.G., Maurotto, A., Tice, D., Lozano-Perez, S., Scenini, F., 2019. Effect of machining on stress corrosion crack initiation in warm-forged type 304L stainless steel in high temperature water. Acta Mater. 165, 203–214. https://doi.org/10.1016/j.actamat.2018.11.046.

Chryssolouris, G., Anifantis, N., Karagiannis, S., 1997. Laser Assisted Machining: an Overview. https://doi.org/10.1115/1.2836822.

Dandekar, C.R., Shin, Y.C., 2010. Laser-assisted machining of a fiber reinforced metal matrix composite. J. Manuf. Sci. Eng. 132 (6) https://doi.org/10.1115/1.4002548.

Davis, J.M., Saei, M., Mohanty, D.P., Udupa, A., Sugihara, T., Chandrasekar, S., 2020. Cutting of tantalum: why it is so difficult and what can be done about it. Int. J. Mach. Tools Manuf. 157, 103607 https://doi.org/10.1016/j.ijmachtools.2020.103607.

Deng, T., Li, J., Zheng, Z., 2020. Fundamental aspects and recent developments in metal surface polishing with energy beam irradiation. Int. J. Mach. Tools Manuf. 148, 103472 https://doi.org/10.1016/j.ijmachtools.2019.103472.

Devillez, A., le Coz, G., Dominiak, S., Dudzinski, D., 2011. Dry machining of Inconel 718, workpiece surface integrity. J. Mater. Process. Technol. 211 (10), 1590–1598. https://doi.org/10.1016/j.jmatprotec.2011.04.011.

Diaz, O.G., Luna, G.G., Liao, Z., Axinte, D., 2019. The new challenges of machining Ceramic Matrix Composites (CMCs): review of surface integrity. Int. J. Mach. Tools Manuf. 139, 24–36. https://doi.org/10.1016/j.ijmachtools.2019.01.003.

Ezugwu, E.O., Bonney, J., Yamane, Y., 2003. An overview of the machinability of aeroengine alloys. J. Mater. Process. Technol.

Gao, Y., Stölken, J.S., Kumar, M., Ritchie, R.O., 2007. High-cycle fatigue of nickel-base superalloy René 104 (ME3): interaction of microstructurally small cracks with grain boundaries of known character. Acta Mater. 55 (9), 3155–3167. https://doi.org/10.1016/j.actamat.2007.01.033.

Herbert, C., Axinte, D.A., Hardy, M., Withers, P., 2014. Influence of surface anomalies following hole making operations on the fatigue performance for a nickel-based superalloy. J. Manuf. Sci. Eng., Trans. ASME 136 (5). https://doi.org/10.1115/1.4027619.

Holmberg, J., Wretland, A., Hammersberg, P., Berglund, J., Suárez, A., Beno, T., 2021. Surface integrity investigations for prediction of fatigue properties after machining of alloy 718. Int. J. Fatigue 144. https://doi.org/10.1016/j.ijfatigue.2020.106059.

Huang, W., Yan, J., 2020. Surface formation mechanism in ultraprecision diamond turning of coarse-grained polycrystalline ZnSe. Int. J. Mach. Tools Manuf. 153, 103554 https://doi.org/10.1016/j.ijmachtools.2020.103554.

Kosai, K., Yan, J., 2020. Effects of cyclic loading on subsurface microstructural changes of zirconia polycrystals in nanoscale mechanical processing. Int. J. Mach. Tools Manuf. 159, 103626 https://doi.org/10.1016/j.ijmachtools.2020.103626.

Li, W., Withers, P.J., Axinte, D., Preuss, M., Andrews, P., 2009. Residual stresses in face finish turning of high strength nickel-based superalloy. J. Mater. Process. Technol. 209 (10), 4896–4902. https://doi.org/10.1016/j.jmatprotec.2009.01.012.

Liao, Z., Axinte, D., Mieszala, M., M'Saoubi, R., Michler, J., Hardy, M., 2018. On the influence of gamma prime upon machining of advanced nickel based superalloy. CIRP Ann. 67 (1), 109–112. https://doi.org/10.1016/j.cirp.2018.03.021.

Liao, Z., Abdelhafeez, A., Li, H., Yang, Y., Diaz, O.G., Axinte, D., 2019. State-of-the-art of surface integrity in machining of metal matrix composites. Int. J. Mach. Tools Manuf. 143, 63–91. https://doi.org/10.1016/j.ijmachtools.2019.05.006.

Liao, Z., Sanchez, I., Xu, D., Axinte, D., Augustinavicius, G., Wretland, A., 2020. Dual-processing by abrasive waterjet machining—A method for machining and surface modification of nickel-based superalloy. J. Mater. Process. Technol. 285 https://doi.org/10.1016/j.jmatprotec.2020.116768.

Liao, Z., la Monaca, A., Murray, J., Speidel, A., Ushmaev, D., Clare, A., Axinte, D., M'Saoubi, R., 2021. Surface integrity in metal machining - Part I: fundamentals of surface characteristics and formation mechanisms. In: International Journal of Machine Tools and Manufacture, vol. 162. https://doi.org/10.1016/j.ijmachtools.2020.103687.

Liu, D., Nguyen, T., Wang, J., Huang, C., 2020a. Mechanisms of enhancing the machining performance in micro abrasive waterjet drilling of hard and brittle materials by vibration assistance. Int. J. Mach. Tools Manuf. 151, 103528 https://doi.org/10.1016/j.ijmachtools.2020.103528.

Liu, Q., Liao, Z., Axinte, D., 2020b. Temperature effect on the material removal mechanism of soft-brittle crystals at nano/micron scale. Int. J. Mach. Tools Manuf. 159, 103620 https://doi.org/10.1016/j.ijmachtools.2020.103620.

Lu, J., Lu, H., Xu, X., Yao, J., Cai, J., Luo, K., 2020. High-performance integrated additive manufacturing with laser shock peening –induced microstructural evolution and improvement in mechanical properties of Ti6Al4V alloy components. Int. J. Mach. Tools Manuf. 148 https://doi.org/10.1016/j.ijmachtools.2019.103475.

Mills, W.J., Brown, C.M., 2001. Fatigue fracture surface morphology for alloy 718. Superalloys 718, 625–706.

Nguyen, D., Tooptong, S., Park, K.H., Kwon, P., 2020. Formation mechanism of alumina layer in protecting cubic boron nitride inserts in turning cast irons. Int. J. Mach. Tools Manuf. 153, 103539 https://doi.org/10.1016/j.ijmachtools.2020.103539.

Novovic, D., Dewes, R.C., Aspinwall, D.K., Voice, W., Bowen, P., 2004. The effect of machined topography and integrity on fatigue life. Int. J. Mach. Tools Manuf. 44 (2–3), 125–134. https://doi.org/10.1016/j.ijmachtools.2003.10.018.

Oh, N.S., Woo, W.S., Lee, C.M., 2018. A study on the machining characteristics and energy efficiency of Ti-6Al-4V in laser-assisted trochoidal milling. Int. J. Prec. Eng. Manuf. - Green Technol. 5 (1), 37–45. https://doi.org/10.1007/s40684-018-0004-y.

Shang, Z., Liao, Z., Sarasua, J.A., Billingham, J., Axinte, D., 2019. On modelling of laser assisted machining: forward and inverse problems for heat placement control. Int. J. Mach. Tools Manuf. 138, 36–50. https://doi.org/10.1016/j.ijmachtools.2018.12.001.

Suárez, Alfredo, Veiga, F., de Lacalle, L.N.L., Polvorosa, R., Lutze, S., Wretland, A., 2016. Effects of ultrasonics-assisted face milling on surface integrity and fatigue life of Ni-Alloy 718. J. Mater. Eng. Perform. 25 (11), 5076–5086. https://doi.org/10.1007/s11665-016-2343-6.

Suárez, A., Veiga, F., Polvorosa, R., Artaza, T., Holmberg, J., de Lacalle, L.N.L., Wretland, A., 2019. Surface integrity and fatigue of non-conventional machined Alloy 718. J. Manuf. Process. 48, 44–50. https://doi.org/10.1016/j.jmapro.2019.09.041.

Tian, Y., Shin, Y.C., 2007. Multiscale Finite Element Modeling of Silicon Nitride Ceramics Undergoing Laser-Assisted Machining. https://doi.org/10.1115/1.2673595.

Toubhans, B., Fromentin, G., Viprey, F., Karaouni, H., Dorlin, T., 2020. Machinability of inconel 718 during turning: cutting force model considering tool wear, influence on surface integrity. J. Mater. Process. Technol. 285 https://doi.org/10.1016/j.jmatprotec.2020.116809.

Umbrello, D., Rotella, G., 2018. Fatigue life of machined Ti6Al4V alloy under different cooling conditions. CIRP Ann. 67 (1), 99–102. https://doi.org/10.1016/j.cirp.2018.03.017.

Wu, D., Zhang, D., Yao, C., 2018. Effect of turning and surface polishing treatments on surface integrity and fatigue performance of nickel-based alloy GH4169. Metals 8 (7). https://doi.org/10.3390/met8070549.

Xu, Z., Dunleavey, J., Antar, M., Hood, R., Soo, S.L., Kucukturk, G., Hyde, C.J., Clare, A. T., 2018. The influence of shot peening on the fatigue response of Ti-6Al-4V surfaces subject to different machining processes. Int. J. Fatigue 111, 196–207. https://doi.org/10.1016/j.ijfatigue.2018.02.022.

Xu, D., Liao, Z., Axinte, D., Hardy, M., 2020a. A novel method to continuously map the surface integrity and cutting mechanism transition in various cutting conditions. Int. J. Mach. Tools Manuf. 151, 103529.

Xu, D., Liao, Z., Axinte, D., Sarasua, J.A., M'Saoubi, R., Wretland, A., 2020b. Investigation of surface integrity in laser-assisted machining of nickel based superalloy. Mater. Des. 194, 108851 https://doi.org/10.1016/j.matdes.2020.108851.

Yang, Z., Zhu, L., Zhang, G., Ni, C., Lin, B., 2020. Review of ultrasonic vibration-assisted machining in advanced materials. Int. J. Mach. Tools Manuf., 103594 https://doi.org/10.1016/j.ijmachtools.2020.103594.

Zhou, J., Bushlya, V., Avdovic, P., Ståhl, J.E., 2012. Study of surface quality in high speed turning of Inconel 718 with uncoated and coated CBN tools. Int. J. Adv. Manuf. Technol. 58 (1–4), 141–151. https://doi.org/10.1007/s00170-011-3374-7.